Ultrasonics 69 (2016) 74–82

Contents lists available at ScienceDirect

Ultrasonics

journal homepage: www.elsevier.com/locate/ultras

Measurement of mechanical quality factors of polymers in flexural vibration for high-power ultrasonic application

Jiang Wu *, Yosuke Mizuno, Marie Tabaru, Kentaro Nakamura

Precision and Intelligence Laboratory, Tokyo Institute of Technology, 4259 Nagatsuta-cho, Midori-ku, Yokohama 226-8503, Japan

ARTICLE INFO

Article history:
Received 9 September 2015
Received in revised form 1 February 2016
Accepted 24 March 2016
Available online 1 April 2016

Keywords:
Polymer
Q factor
Flexural vibration
High-power ultrasonic application

ABSTRACT

A method for measuring the mechanical quality factor (*Q* factor) of materials in large-amplitude flexural vibrations was devised on the basis of the original definition of the *Q* factor. The *Q* factor, the ratio of the reactive energy to the dissipated energy, was calculated from the vibration velocity distribution. The bar thickness was selected considering the effect of the thickness on the estimation error. In the experimental setup, a 1-mm-thick polymer-based bar was used as a sample and fixed on the top of a longitudinal transducer. Using transducers of different lengths, flexural waves in the frequency range of 20–90 kHz were generated on the bar. The vibration strain in the experiment reached 0.06%. According to the Bernoulli–Euler model, the reactive energy and dissipated energy were estimated from the vertical velocity distribution on the bar, and the *Q* factors were measured as the driving frequency and strain were varied. The experimental results showed that the *Q* factors decrease as the driving frequencies and strains increase. At a frequency of 28.30 kHz, the *Q* factor of poly(phenylene sulfide) (PPS) reached approximately 460 when the strain was smaller than 0.005%. PPS exhibited a much higher *Q* factor than the other tested polymers, which implies that it is a potentially applicable material as the elastomer for high-power ultrasonic devices.

1. Introduction

Metallic compounds, such as stainless steels and aluminum alloys, are commonly used as elastomers in ultrasonic transducers. To obtain high vibration velocities with lightweight transducers, a material with low elastic modulus, low density, and low mechanical loss is required as the elastomer. Among existing functional materials, polymers usually have low elastic moduli and densities. It has been believed that, in most cases, polymers are good at absorbing vibrations because of their high mechanical loss. However, some of the new functional polymers invented in the last three decades exhibit low mechanical loss. To gain a primary understanding of the mechanical-loss properties of polymers, it is of significance to evaluate the mechanical loss under ultrasonic frequencies and large amplitudes. As flexural vibrations are widely used in ultrasonic transducers [1–8], in this study, we focus on the mechanical-loss properties of polymers in flexural vibrations.

The mechanical quality factor (*Q* factor) is inversely proportional to the mechanical loss, and it is a commonly-used parameter that indicates the suitability of a material as a vibrator. Many methods for *Q*-factor measurement have been developed: (1) Impact testing method is being widely applied in industry [9]. The *Q* factor is obtained from the decay in the damped oscillation curve at the natural frequency of the sample after striking it with a hammer. (2) The resonance curve method is used to evaluate the mechanical loss of transducers [4]. The *Q* factor is calculated from the curve of vibration amplitude versus frequency, which provides an overall result originating from the loss in the elastomer, loss in the excitor (e.g. piezoelectric ceramic elements), and loss generated on the contacting surface between the elastomer and the excitor. (3) The *Q* factor can be derived from the attenuation coefficient of a traveling wave. The attenuation coefficient is calculated from the amplitude ratio of reflected waves that are generated by a burst excitation [10]. However, the vibration amplitude is limited because of the low power of the burst excitation. (4) The attenuation coefficient can be directly calculated from the fitting curve of the distance decay of a traveling wave generated by a continuous excitation. However, it is difficult to separate the traveling wave from the reflected wave on a vibrating bar, especially for a material with low mechanical loss.

A method that gives a precise value of the *Q* factor (or attenuation coefficient) of polymers under ultrasonic frequencies and large amplitudes is required. In a previous study [11], a method for measuring the *Q* factors of a cylindrical bar in torsional vibration was

* Corresponding author. Tel.: +81 45 924 5052; fax: +81 45 924 5091.
E-mail address: wujiang@sonic.pi.titech.ac.jp (J. Wu).

http://dx.doi.org/10.1016/j.ultras.2016.03.012
0041-624X/

developed. The Q factors were calculated from the torsional vibration velocity distribution on the side surface based on the original definition of the Q factor. In the present work, we modify the aforementioned method to measure the Q factor in flexural vibration. In addition, we discuss the requirements for achieving high measurement precision. When the frequencies and strains are varied, we measure the Q factors of bars made of polyacetal (POM), acryloni trile–butadiene–styrene (ABS), poly(ether ether ketone) (PEEK), and poly(phenylene sulfide) (PPS).

2. Principle of Q-factor measurement

2.1. Original definition of Q factor

Fig. 1(a) shows a vibrating bar. Flexural waves are generated with a vibration source located at one end. The original definition of the Q factor is the ratio of the reactive energy E_k to the dissipated energy E_p in the sampling part between the cross-sections L_1 and L_2:

$$Q = \frac{2\pi E_k}{E_p}. \tag{1}$$

The reactive energy stored in the vibrating bar consists of kinetic energy and elastic energy. In the time domain, they are transforming to each other and their sum is constant [12]. Thus, the reactive energy equals the maximum kinetic energy. The displacement of a small section is a composition of a translational motion in the vertical direction and a rotation [13]. Thus, the maximum kinetic energy is given as

$$\begin{aligned} E_k &= \int_{L_1}^{L_2} d\left(\frac{1}{2}mv^2\right) + \int_{L_1}^{L_2} d\left(\frac{1}{2}I\varphi^2\right) \\ &= \frac{1}{2}\rho bh\int_{L_1}^{L_2} v^2 dz + \frac{1}{24}\rho bh^3\int_{L_1}^{L_2}\varphi^2 dz, \end{aligned} \tag{2}$$

where v and φ represent the zero-to-peak vertical velocity and angular velocity, respectively. m and I are the mass and rotary inertia of the sampling interval, respectively. ρ is the density, and b and h represent the width and thickness of the specimen, respectively. The rotary inertia I is determined by the width and thickness as $I = bh^3/12$.

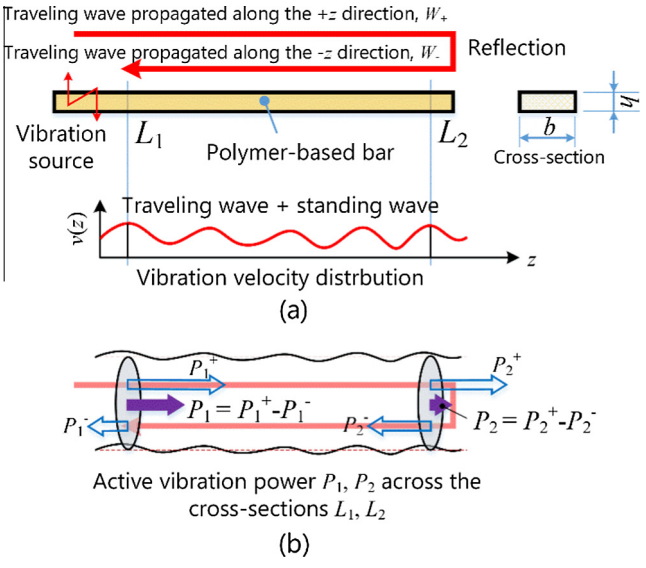

Fig. 1. Q-factor measurement from the vibration velocity distribution. (a) The wave, consisting of a traveling wave and a standing wave, is generated on the vibrating bar. A composition of two traveling waves, W_+ and W_-, with inverse propagation directions is assumed. (b) P_1^+ and P_1^- are the active vibration powers of W_+ and W_- across L_1, respectively, and $P_1 = P_1^+ - P_1^-$. P_2^+ and P_2^- are the active vibration powers of W_+ and W_- across L_2, respectively, and $P_2 = P_2^+ - P_2^-$.

The dissipated energy E_p is the decrease in the active vibration energy flowing across L_1 and L_2:

$$E_p = \frac{2\pi}{\omega_0}\cdot(P_1 - P_2), \tag{3}$$

where ω_0 is the angular frequency, and P_1 and P_2 represent the active vibration powers of the wave flowing across L_1 and L_2, respectively. If the wave amplitude decreases to zero before reflection because of large energy dissipation, only a traveling wave exists on the bar, and it is clear that E_p exceeds zero. In most cases, a wave that consists of a traveling wave and a standing wave is generated. It is necessary to investigate whether Eq. (3) is effective in calculating the dissipated energy of this wave. We assume that the wave in Fig. 1(a) is a combination of a traveling wave propagating along the $+z$ axis, W_+, and a traveling wave propagating along the $-z$ axis, W_-. Further, W_- is the reflected wave of W_+. In Fig. 1 (b), P_1^+ represents the active vibration power of W_+ flowing across L_1, and its positive direction is along the $+z$ axis. On the other hand, P_1^- is the active vibration power of W_- that flows across L_1, and its positive direction is along the $-z$ axis. When W_+ and W_- flow across L_1 simultaneously, the active vibration power P_1 equals $P_1^+ - P_1^-$. Similarly, P_2^+ and P_2^- represent the active vibration powers of W_+ and W_- flowing across L_2, and $P_2 = P_2^+ - P_2^-$. Thus, Eq. (3) can be rewritten as

$$E_p = \frac{2\pi}{\omega_0}\cdot\left[\left(P_1^+ - P_1^-\right) - \left(P_2^+ - P_2^-\right)\right] = \frac{2\pi}{\omega_0}\cdot\left[\left(P_1^+ - P_2^+\right) + \left(P_2^- - P_1^-\right)\right], \tag{4}$$

where $P_1^+ - P_2^+$ and $P_2^- - P_1^-$ represent the dissipated powers of W_+ and W_-, respectively. Because W_+ flows across L_1 and L_2 successively, P_1^+ is larger than P_2^+ owing to energy dissipation during propagation. Similarly, P_2^- is larger than P_1^-. Since W_- is the reflection wave of W_+, P_2^+ is larger than P_2^-. Thus, E_p exceeds zero, which indicates that Eq. (3) is effective in calculating the dissipated energy when a traveling wave and a standing wave are generated simultaneously. In the experiments for Q-factor measurement described later, as high-amplitude vibrations are generated on long polymer-based bars, the active vibration power and dissipated power are measureable. Note that it is difficult to estimate Q factors of materials with extremely low mechanical loss, such as sapphire [14], for which P_1^+ equals P_1^- approximately, and P becomes too small to be detected.

In an alternating current circuit, the active power (or real power) P is calculated from the zero-to-peak voltage u and current i [12]:

$$P = \frac{1}{2}Re(u\cdot i^*). \tag{5}$$

The voltage u and current i are given as complex numbers; Re represents the real part and the asterisk indicates the complex conjugate. The active power in a mechanical system is calculated from the force (moment) and the translational velocity (angular velocity), which correspond to the voltage and current in an electrical system, respectively. The active vibration power in flexural vibration is calculated as [15–17]

$$P = \frac{1}{2}Re(V\cdot v^* - M\cdot\varphi^*), \tag{6}$$

where V and M represent the shearing force and bending moment acting on the cross-section, respectively. The active vibration power consists of the shearing-force component $V\cdot v^*$ and the bending-moment component $-M\cdot\varphi^*$. The shearing-force component is $V\cdot v^*$, because the positive direction of V on the right lateral surface of the bar element (Fig. 2(a)) is $+y$ axis, which is the same as that of v. The bending-moment component equals $-M\cdot\varphi^*$ because the

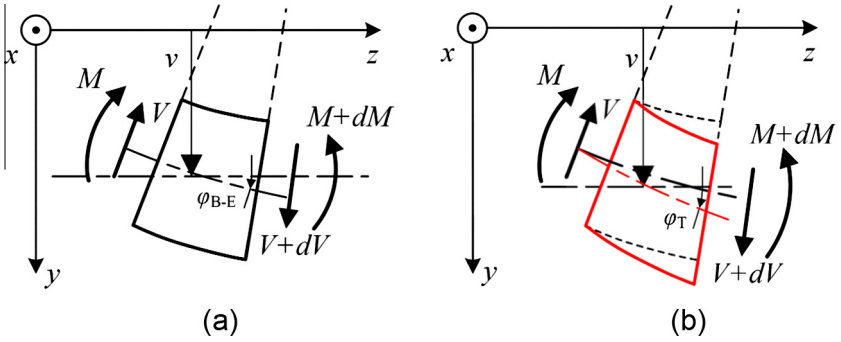

Fig. 2. The mechanical models for describing the flexural deformation on a bending bar. (a) The Bernoulli–Euler model and (b) the Timoshenko model.

positive directions of M and φ are along the $+x$ and $-x$ axis, respectively. The zero-to-peak vertical velocity v is measured directly at different positions along the z axis. The rotation angle φ, shear force V, and bending moment M need to be theoretically derived from the vertical velocity v. The Bernoulli–Euler model, as shown in Fig. 2(a), is valid for a bar of small thickness. The Timoshenko model, as shown in Fig. 2(b), is an improved version of the Bernoulli–Euler model, and it describes the flexural deformation of a thick bar more precisely [13,18]. Because the deformations generated by the shearing force and rotary inertia are taken into account, the rotation angle estimated by the Timoshenko model is larger than that estimated by the Bernoulli–Euler model under the same driving force [17]. However, the calculation in the Timoshenko model is more complicated. To obtain high precision with low calculation cost, choosing a thin sample bar that is valid under the Bernoulli–Euler model is a reasonable approach. To determine the appropriate thicknesses of the sample bars, the error in the Bernoulli–Euler model is estimated quantitatively.

2.2. Comparison of Q factors calculated using Bernoulli–Euler model and Timoshenko model

According to the Bernoulli–Euler model, the rotation angle φ, shearing force V, and bending moment M for the vertical velocity v are given as

$$\varphi = \frac{dv}{dz}, \tag{7}$$

$$\frac{dV}{dt} = EI_z \cdot \frac{d^3 v}{dz^3}, \tag{8}$$

$$\frac{dM}{dt} = EI_z \cdot \frac{d^2 v}{dz^2}, \tag{9}$$

where E is the elastic modulus and I_z is the second moment of area. For a rectangular cross-section, I_z is determined by the width and thickness as $I_z = bh^3/12$. In the Timoshenko model, the rotation angle φ, shearing force V, and bending moment M are given as [17]

$$\varphi = \frac{dv}{dz} + \frac{V}{\kappa GA}, \tag{10}$$

$$\frac{dV}{dz} = \rho A \cdot \frac{dv}{dt}, \tag{11}$$

$$\frac{dM}{dz} = V + \rho I_z \cdot \frac{d\varphi}{dt}, \tag{12}$$

where A, the cross-sectional area, is determined by the width and thickness as $A = bh$. G represents the shear modulus. κ is the Timoshenko coefficient for a rectangular cross-section, and it is determined by Poisson's ratio μ [17]:

$$\kappa = \frac{10(1+\mu)}{12+11\mu}. \tag{13}$$

Considering that the wave is reflected at the free end of the bar, we assume a harmonic solution for the wave equation as

$$v(t,z) = A_0\{\exp[j\omega_0 t - (\alpha + jk)\cdot z] + \exp[j\omega_0 t + (\alpha + jk)\cdot(z - 2l)]\}, \tag{14}$$

where A_0 is the amplitude of the vibration velocity, α is the attenuation coefficient, k is the wavenumber, and l is the total length of the vibrating bar. As the length was varied from 0 to 1.5 times the wavelength, the Q factors were calculated on the basis of the Bernoulli–Euler model and the Timoshenko model, as Q_{B-E} and Q_T, respectively. Assuming that the Q factor calculated by the Timoshenko model gives a precise value, the error in the Bernoulli–Euler model is given as

$$e = 1 - \frac{Q_{B-E}}{Q_T}. \tag{15}$$

Considering the measurement results in the previous study [19], the attenuation coefficient was varied from 0.03 to 60 dB/cm in our simulation. The other parameters are listed in Table 1. Fig. 3(a) and (b) shows the results for attenuation coefficients of 0.03 and 30 dB/cm, respectively. In Fig. 3(a), Q_{B-E} reached 1040, which was smaller than Q_T. This is mainly attributed to the large reactive energy calculated by the Timoshenko model. As stated above, under the same driving force, the rotation angle calculated by the Timoshenko model is larger than that calculated by the Bernoulli–Euler model. Thus, the reactive energy increases as the rotation angle increases. Fig. 3(b) shows that, at an attenuation coefficient of 30 dB/cm, both Q_{B-E} and Q_T were less than 2. The dissipated energy increases with the attenuation, resulting in a decrease in the Q factor.

Fig. 4 shows the Q_{B-E}-to-Q_T ratios when the attenuation coefficients are 0.03, 0.3, 3, 30, and 60 dB/cm. The Q_{B-E}-to-Q_T ratio was determined by both the attenuation coefficient and the thickness-to-wavelength ratio. When the attenuation coefficient was varied from 0.03 to 0.3 dB/cm, the Q_{B-E}-to-Q_T ratio did not change significantly. In contrast, the Q_{B-E}-to-Q_T ratio tended to 1 as the attenuation increased. When the thickness-to-wavelength ratio was 0.2, the error was smaller than 0.2%. When the

Table 1
Parameters used in simulation.

Parameter	Unit	Value
Elastic modulus, E	GPa	3.45
Density, ρ	$\times 10^3$ kg/m^3	1.35
Poisson's ratio	–	0.36
Width, b	mm	10
Length, l	mm	500
Wavenumber, k	mm^{-1}	0.628

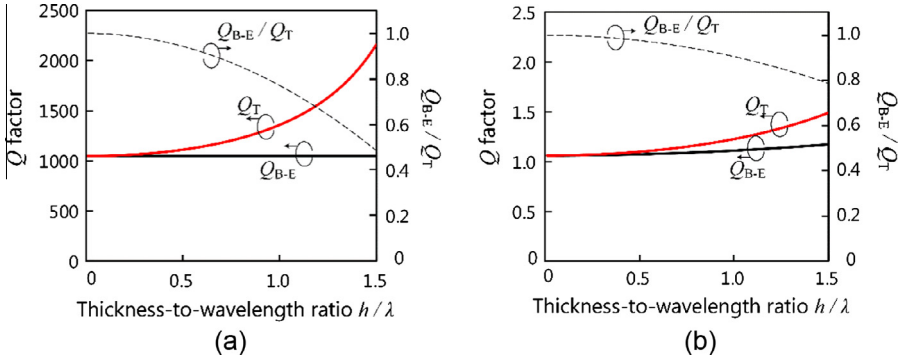

Fig. 3. Q factors calculated by the Bernoulli–Euler model (Q_{B-E}), the Timoshenko model (Q_T), and the Q_{B-E}-to-Q_T ratio as a function of the thickness-to-wavelength ratio, h/λ, at attenuations of (a) 0.03 dB/cm and (b) 30 dB/cm.

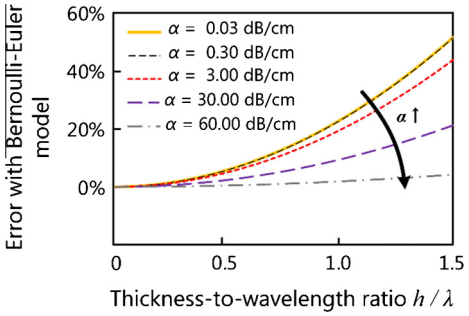

Fig. 4. Error in the Bernoulli–Euler model as a function of the thickness-to-wavenumber ratio, h/λ, at attenuations of 0.03, 0.3, 3, 30.00, and 60.00 dB/cm.

thickness-to-wavelength ratio increased to 0.5, the error increased to approximately 5% at an attenuation coefficient of 0.03 dB/cm.

In summary, the error in the Bernoulli–Euler model is smaller for a material with high mechanical loss. The maximum error is smaller than 0.2% if the thickness is less than 0.2 times the wavelength when the attenuation coefficients of the tested polymers are greater than 0.03 dB/cm. Based on the simulation results, we will discuss the appropriate thickness of the bar later.

3. Experimental setup

3.1. Sample polymers

In this study, the Q factors of some functional polymers, namely, POM, ABS, PEEK, and PPS, were experimentally investigated. In industrial applications, lightweight gears are usually made of POM because of its high resistance to abrasion and heat [20]. ABS has good flowability and high resistance to impact [21]. The current version of PEEK has excellent abrasion resistance and workability [22,23]. PPS is widely employed in the automotive and electrical industries because PPS has good wear properties [24]. The elastic moduli, densities and Poisson's ratios of POM, ABS, PEEK, and PPS tested in the experiments are listed in Table 2.

Table 2
Mechanical parameters of the tested polymers.

Polymer	Elastic modulus, E (GPa)	Density, ρ ($\times 10^3$ kg/m^3)	$\sqrt{E/\rho}$ ($\times 10^3$ m/s)	Poisson's ratio, μ
POM	2.80	1.41	1.41	0.35
ABS	2.40	1.05	1.51	0.36
PEEK	3.50	1.28	1.65	0.40
PPS	3.45	1.35	1.59	0.36

3.2. Experimental setup

Fig. 5 shows the experimental setup for Q-factor measurements of the polymer samples. Piezoelectric longitudinal transducers with resonance frequencies of 30, 42, 65, and 95 kHz were prepared to generate ultrasonic-frequency vibrations. One end of the bar was fixed at the top of the transducer with a bolt. When a driving voltage was applied to the piezoelectric ceramic elements in the longitudinal transducer, a flexural wave was generated on the bar. The strain on the vibrating bar was changed by adjusting the amplitude of the driving voltage. A laser Doppler velocimeter (NLV1232, Polytec, Waldbronn, Germany) mounted on a guide rail was used to record the vertical velocities on the bar surface at different positions. The amplitude of the vibration velocity and the phase between the velocity and the input signal were detected with a lock-in voltmeter (5560, NF electronic instruments, Yokohama, Japan).

3.3. Appropriate thicknesses of polymer-based vibrating bars

To determine the appropriate thickness for the Bernoulli–Euler model, we calculated the wavelength of the flexural waves using the expression [17]:

$$\lambda^2 = \frac{2\pi}{f}\sqrt{\frac{EI_z}{\rho A}} = 1.814 \cdot \frac{h}{f} \cdot \sqrt{\frac{E}{\rho}}, \tag{16}$$

where f is the driving frequency. Substituting the elastic modulus and density of PPS into Eq. (16), the wavelengths of the PPS-based bars were calculated as a function of thickness at 30, 42, 65, and 95 kHz. Fig. 6 shows the results. When the thickness was 1 mm and the frequency was 95 kHz, the wavelength was approximately 5.5 mm and the thickness-to-wavelength ratio was approximately 0.18. When the frequency decreased to 30 kHz, the thickness-to-wavelength ratio decreased to 0.1 monotonically. According to the simulation results in Fig. 4, the error in the Bernoulli–Euler model was smaller than 0.2% if the thickness-to-wavelength ratio was varied from 0.1 to 0.18, which can be tolerated in this measurement. When the thickness increased to 3 mm, the thickness-to-wavelength ratio reached 0.31 at 95 kHz and the error increased to 2% for a material with low mechanical loss. Fig. 6 is also effective in determining the appropriate thicknesses of the POM-, ABS-, and PEEK-based vibrating bars, because the tested polymers do not differ significantly in terms of their elastic moduli and densities. Considering the workability, polymer samples of 1 mm in thickness, 10 mm in width, and 300 mm in length were used in this study. The theoretical error in the Bernoulli–Euler model is 0.2%.

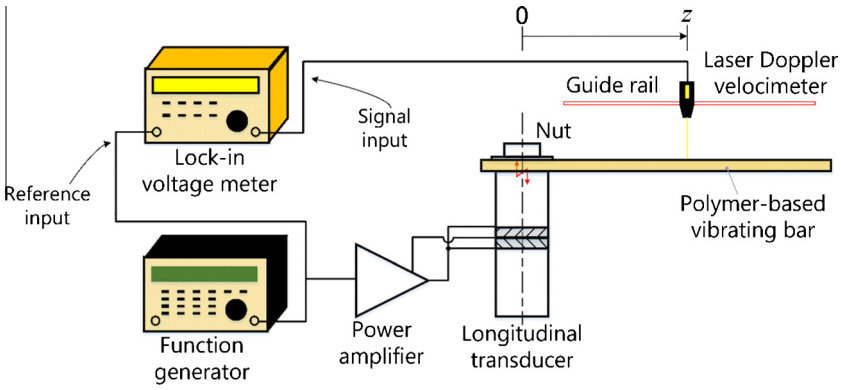

Fig. 5. Experimental setup for Q factor measurement by the devised method.

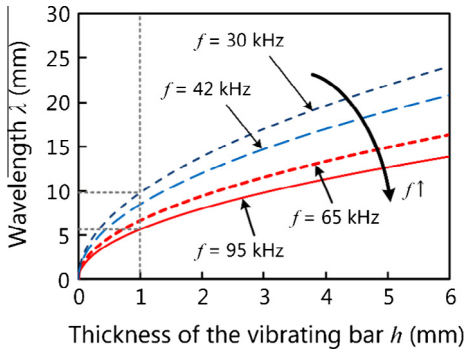

Fig. 6. Wavelength, λ, of the flexural wave for the PPS-based vibrating bar as a function of the thickness, h.

3.4. Measurement procedure

To calculate the Q factor from the discrete measurement results of the vibration velocity distribution, Eqs. (2) and (6)–(9) need to be discretized. In previous studies [14–16], the data was processed in the wavenumber space (k space) to suppress the error generated in high-order finite difference calculations. The procedures are as follows:

(1) Implementing the spatial Fourier transform, the k-space spectrum $\Gamma_{\mathrm{raw}}(k)$ of the vibration velocity distribution $v(z)$ is obtained.

(2) A low-pass filter is employed in the k space to reduce the noise of the high-wavenumber components. The function of the low-pass filter $L(k)$ is given as [15]

$$L(k)=\begin{cases}1-\frac{1}{2}\exp\left\{-S\cdot\left[1-\left(\frac{k}{k_c}\right)^2\right]\right\}, & k\leqslant k_c,\\ \frac{1}{2}\exp\left\{-S\cdot\left[\left(\frac{k}{k_c}\right)^2-1\right]\right\}, & k>k_c,\end{cases} \tag{17}$$

where k_c is the cutoff wavenumber and S is the filter-shape coefficient. The optimal values of k_c and S have been investigated in a previous study [14]: the ratio of the cutoff wavenumber k_c to the propagating wavenumber k_0 was set to 1.8 and the filter-shape coefficient S was set to 10. The filtered k-space spectrum $\Gamma(k)$ is given as

$$\Gamma(k)=L(k)\cdot\Gamma_{\mathrm{raw}}(k). \tag{18}$$

(3) Substituting Eqs. (7)–(9) into Eq. (6), and implementing discretization, the active vibration power flow is given as

$$P(z)=\frac{EI_z}{2\omega_0}\cdot\mathrm{Im}\left[\frac{d^3v(z)}{dz^3}\cdot v^*(z)-\frac{d^2v(z)}{dz^2}\cdot\frac{dv^*(z)}{dz}\right]. \tag{19}$$

The 1st-, 2nd-, and 3rd-order spatial derivatives of the vibration velocities are calculated in the k space using the expression [14]:

$$\Gamma_n(k)=\Gamma\left[\frac{d^nv}{dz^n}\right]=(jk)^n\cdot\Gamma(k), \tag{20}$$

where n represents the order of the derivative and $\Gamma_n(k)$ is defined as the k-space spectrum of the nth-order derivative of the filtered vibration velocity. Using the inverse spatial Fourier transform, the filtered vibration velocity distribution v_f, and the 1st-, 2nd-, and 3rd-order derivatives of the vibration velocity (dv/dz, d^2v/dz^2, and d^3v/dz^3) are calculated from $\Gamma(k)$, $\Gamma_1(k)$, $\Gamma_2(k)$, and $\Gamma_3(k)$, respectively.

(4) The reactive-energy distribution $\Delta E_k(z)$ and the local-dissipated-power distribution $\Delta P(z)$ are given as

$$\Delta E_k(z)=\frac{1}{2}\rho bh\cdot v^2(z)\cdot\Delta z+\frac{1}{24}\rho bh^3\cdot\left[\frac{dv(z)}{dz}\right]^2\cdot\Delta z, \tag{21}$$

$$\Delta P(z)=P(z)-P(z+\Delta z), \tag{22}$$

where Δz is the sampling interval along the z axis, which is set to 0.1 times the wavelength in this study. The reactive energy E_k and dissipated energy E_p between L_1 and L_2 are given as

$$E_k=\sum_{L_1}^{L_2}\Delta E_k(z), \tag{23}$$

$$E_p=\frac{2\pi}{\omega_0}\sum_{L_1}^{L_2}\Delta P(z). \tag{24}$$

(5) Finally, the Q factors are calculated with Eq. (1).

4. Experimental results

4.1. Dissipated power

Fig. 7(a) shows the vibration velocity distribution on the PPS-based bar at a frequency of 28.30 kHz and driving voltage of 100 V. The maximum vibration velocity reached 280 mm/s. The spectrum of the vibration velocity is shown Fig. 7(b). The propagating wavenumber k_0 was approximately 0.616 mm^{-1} (λ = 10.2 mm) at 28.30 kHz. The cut-off wavenumber of the low-pass filter was set to 0.9 mm^{-1}. Fig. 7(c) and (d) shows the reactive-energy distribution $\Delta E_k(z)$ and the local-dissipated-energy distribution $\Delta P(z)$ along the z axis. Clearly, the reactive energy and the local

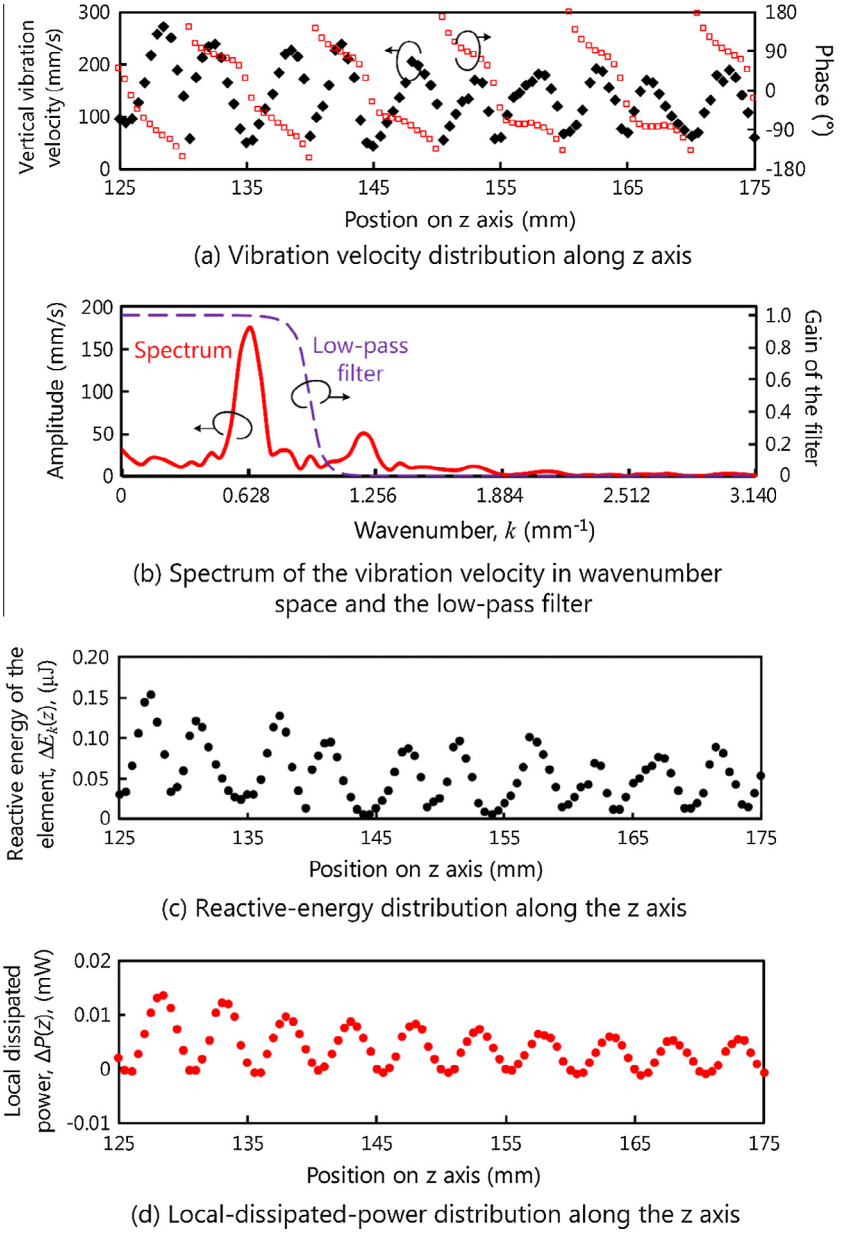

Fig. 7. Example of Q-factor calculation. (a) Vibration velocity distribution at a driving frequency of 28.30 kHz and zero-to-peak voltage of 100 V. (b) Spectrum of the vibration velocity and the low-pass filter. (c) Reactive-energy distribution, $\Delta E_k(z)$, and (d) local-dissipated-power distribution, $\Delta P(z)$, along the z axis.

dissipated energy decreased as the propagating distance increased. In this study, the integral interval (L_1–L_2) for calculating E_k and E_p were 125–175 mm.

Based on the Bernoulli–Euler model [13,18], the strain γ on the bending bar is given as

$$\gamma = \frac{M}{EI_z} \cdot \frac{h}{2}. \tag{25}$$

Substituting Eq. (9) into Eq. (25), we obtain

$$\gamma = \frac{h}{2\omega_0} \cdot \frac{d^2 v}{dz^2}. \tag{26}$$

The 2nd-order derivative of the vibration velocity was obtained using Eq. (20). The maximum strain of the 1-mm-thick PPS-based bar in the range of 125–175 mm is 0.037%. Using Eqs. (23) and (24), we calculated that the reactive energy and dissipated energy in the range of 125–175 mm are 4.900×10^{-6} J and 0.085×10^{-6} J, respectively. Thus, the Q factor of PPS is 362 at a driving frequency of 28.30 kHz and strain of 0.037%.

4.2. Q factors of the tested polymers

Fig. 8 shows the Q factors of the PPS-, PEEK-, POM-, and ABS-based bars as the strain is varied from 0.005% to 0.060% at 40.99 kHz. The Q factor of the PPS-based bar was approximately 350 at 0.005%. As the strain increased, the Q factors of the PPS-, PEEK-, POM-, and ABS-based bars decreased. The Q factor of the PPS-based vibrating bar decreased to approximate 150 at 0.058%, which was 0.4 times that at 0.005%. The Q factor of the PEEK-based bar was approximately 90 at 0.006%. The Q factors of the POM- and ABS-based bars were approximately 20, which were only 0.06 times the maximum Q factor of the PPS-based bar.

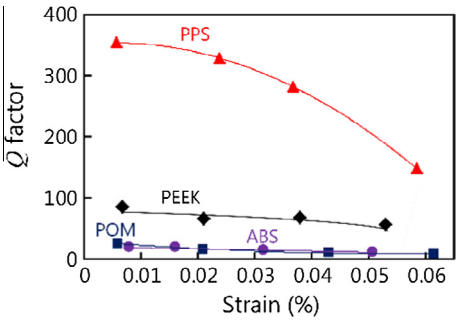

Fig. 8. Q factors of the PPS-, PEEK-, POM-, and ABS-based vibrating bars as a function of the strain at a frequency of 40.99 kHz.

Fig. 9(a) shows the Q factors of the PPS-based bar versus the strain at 28.30, 40.99, 63.84, and 90.23 kHz. The maximum Q factor reached approximately 460 at a driving frequency of 28.30 kHz and strain of 0.050%. The attenuation coefficient corresponding to the maximum Q factor was approximately 0.05 dB/cm. When the strain was smaller than 0.020%, the Q factors did not change significantly. In contrast, the Q factors decreased sharply when the strain exceeded 0.020%, especially at 28.30 and 40.99 kHz. As shown in Fig. 9(b), the maximum Q factor of the PEEK-based vibrating bar was 115 and decreased as the strain increased.

Fig. 10 shows the Q factors of the PPS- and PEEK-based bars as a function of the driving frequency when the strains are 0.005–0.010% and 0.035–0.040%. The Q factors of the PPS- and PEEK-based bars decreased as the driving frequency increased. The fitting curves show that the Q factor is inversely proportional to the driving frequency in the range of 30–100 kHz. The decrease in the Q factors with increasing vibration velocity and driving frequency may be attributed to the hysteretic strain–stress behavior of polymers [19,25].

We draw the following conclusions about the Q factors of the tested polymers: (1) The Q factors of the polymer-based vibrating bars decrease as the vibration velocity and driving frequency increase. (2) When the driving frequency is 28.30 kHz and he strain is smaller than 0.005%, the Q factor of the PPS-based vibrating bar reaches 460, which is larger than those of other tested polymers under the same strain and driving frequency.

4.3. Comparison with experimental results obtained via impact testing

For comparison, the Q factors of the PPS- and PEEK-based cantilevers were also measured using the impact testing method [9]. The experimental setup is shown in Fig. 11. Cantilevers with lengths of 100, 150, and 200 mm were sandwiched between two

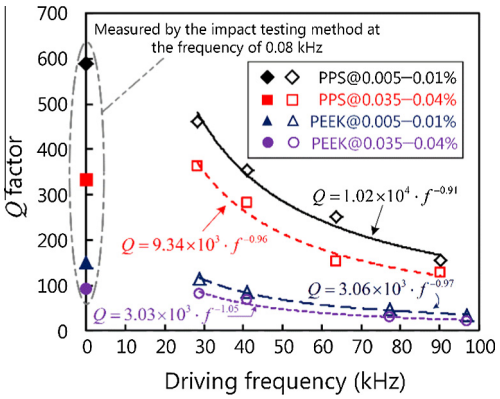

Fig. 10. Q factors of the PPS- and PEEK-based bars as a function of the driving frequency in the strain ranges of 0.005–0.01% and 0.035–0.04%. The Q factors of the PPS- and PEEK-based vibrating bars at a natural frequency of 0.08 kHz are measured by the impact testing method.

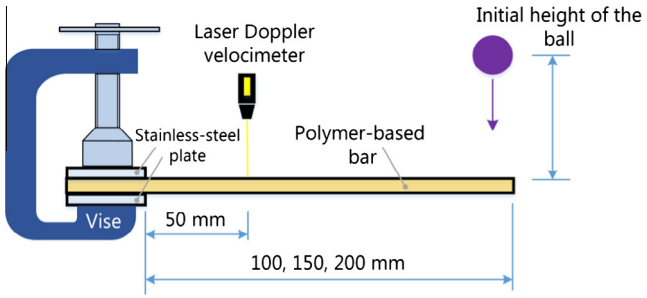

Fig. 11. Experimental setup for Q-factor measurement by the impact testing method.

stainless-steel plates with a vise. The width and thickness of the cantilevers were 10 and 1 mm, respectively. A 20-mm-diameter ball made of stainless steel was released from the position above the free end of the cantilever to give a transient mechanical input. The strain on the cantilever was changed by adjusting the initial height of the ball. The laser Doppler velocimeter (see Section 3.2) was used to measure the vibration velocity at 50 mm from the fixed end. In theory, the vibration velocity on the vibrating bar is a damped oscillation with an exponential envelope, which is given as

$$v(t) = V_0 \cdot e^{-\zeta\omega_n t} \cdot \sin(\omega_n t + \theta), \tag{27}$$

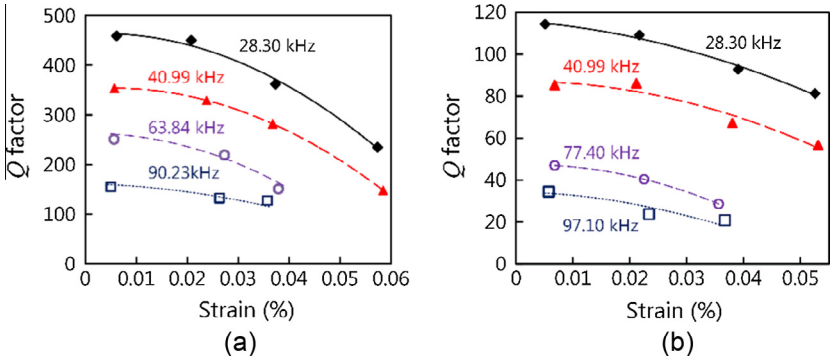

Fig. 9. Q factors of (a) the PPS-based and (b) PEEK-based vibrating bars as a function of the strain.

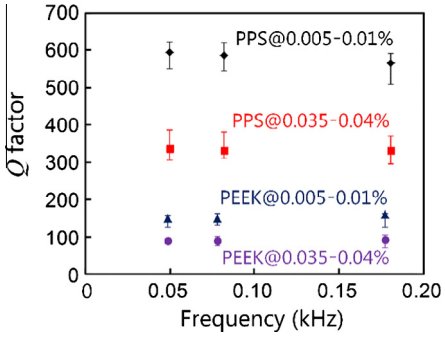

Fig. 12. Q factors of the PPS- and PEEK-based bars measured by the impact testing method.

where V_0, 2ζ, ω_n, and θ represent the initial vibration velocity, damping coefficient, natural frequency of the bar, and phase, respectively. The Q factor is given as [12]

$$Q = \frac{1}{2\zeta}. \tag{28}$$

The Q factor was calculated by fitting the measured data with the envelope of Eq. (27). The measurements were carried out 20 times and the averaged value was selected as the Q factor of the polymer at a certain strain.

Fig. 12 shows the Q factors measured by the impact testing method. The natural frequencies of the 100-, 150-, and 200-mm-long polymer-based bars were approximately 0.18, 0.08, and 0.05 kHz, respectively. In the range of 0.005–0.010%, the Q factor of the PPS-based cantilever was approximately 580, which was twice as high as that in the range of 0.035–0.040%. The Q factor of the PEEK-based cantilever was 150 in the range of 0.005–0.010% and decreased to 90 as the strain increased to 0.040%. The experimental results also demonstrate that the Q factor is independent of frequency in the range of 0.050–0.180 kHz.

The Q factors of the PPS- and PEEK-based bars at 0.08 kHz measured using the impact tested method are shown in Fig. 10. They are in accordance with the frequency- and strain-dependences of the Q factor measured by the devised method described above. However, these Q factors are lower than the values extrapolated from the results obtained by the devised method. This may be attributed to the mechanical loss generated on the contacting surface between the cantilever and the plates. In the devised method (Fig. 5), the energy loss is distributed in the transducer, contacting surface, and polymer-based bar. Since the active vibration power flowing across a cross-section is calculated, the dissipated energy, which reflects the energy loss generated on a certain part, can be estimated. In contrast, using the impact testing method (Fig. 11), it is difficult to separate the energy loss generated on the bar from that on the contacting surface between the plate and the polymer-based bar. In the impact testing method, the energy loss in the vibration system is used as the dissipated energy in calculations, which yields a smaller Q factor than that obtained by the devised method.

5. Conclusions

As the first step in investigating the possibility of employing polymers as elastomers in high-power ultrasonic applications, we devised a method for evaluating the mechanical loss in ultrasonic frequencies and high vibration amplitudes, and we measured the Q factors of some functional polymers. Based on its original definition, the Q factor was precisely measured for a bar with sufficiently small thickness. The Q factor decreased as the driving frequencies and strains increased. At 28.30 kHz, the Q factor of PPS reached approximately 460 when the strain on the bar was smaller than 0.005%, which indicated that PPS can be potentially employed as an elastomer in ultrasonic transducers. In the future, using this method, we will explore the mechanical loss of other functional polymers.

Acknowledgement

The authors thank the Daicel Corporation for providing some polymer samples in this study.

References

[1] M. Takano, M. Takimoto, K. Nakamura, Electrode design of multilayer piezoelectric transducer for longitudinal-bending ultrasonic actuators, Acoust. Sci. Technol. 32 (3) (2011) 100–108.
[2] T. Morita, M.K. Kurosawa, T. Higuchi, Cylindrical micro ultrasonic motor utilizing bulk lead zirconate titanate (PZT), Jpn. J. Appl. Phys. 38 (5B) (1999) 3347–3350.
[3] D. Koyama, Y. Wada, K. Nakamura, M. Nishikawa, T. Nakagawa, H. Kihara, An ultrasonic air pump using an acoustic traveling wave along a small air gap, IEEE Trans. Ultrason. Ferroelectr. Freq. Control 57 (1) (2010) 253–261.
[4] T. Morita, M.K. Kurosawa, T. Higuchi, A cylinder shaped micro ultrasonic motor utilizing PZT thin film (1.4 mm in diameter and 5.0 mm long stator transducer), Sens. Actuat. A – Phys. 83 (1-3) (2000) 225–230.
[5] W. Manthey, N. Kroemer, V. Magori, Ultrasonic transducers and transducer array for application in air, Meas. Sci. Technol. 3 (3) (1992) 249–261.
[6] A. Barone, J.A. Gallego-Juárez, Flexural vibrating free-edge plates with stepped thickness for generating high directional ultrasonic radiation, J. Acoust. Soc. Am. 51 (3) (1972) 954–959.
[7] M. Tabaru, M. Nakazawa, K. Nakamura, S. Ueha, Three-axis acceleration sensor using polyurea films, Jpn. J. Appl. Phys. 47 (5) (2008) 4044–4047.
[8] J. Wu, Y. Mizuno, M. Tabaru, K. Nakamura, Ultrasonic motors with polymer-based vibrators, IEEE Trans. Ultrason. Ferroelectr. Freq. Control 62 (12) (2015) 2169–2178.
[9] T.J. Schultz, Alternative test method for evaluating impact noise, J. Acoust. Soc. Am. 60 (3) (1976) 645–655.
[10] E.P. Papadakis, Traveling wave reflection methods for measuring ultrasonic attenuation and velocity in thin rods and wires, J. Appl. Phys. 42 (7) (1971) 2990–2995.
[11] K. Nakamura, K. Kakihara, M. Kawakami, S. Ueha, Measuring vibration characteristics at large amplitude region of material for high power ultrasonic vibration system, Ultrasonics 38 (1–8) (2000) 122–126.
[12] B.F. Ley, S.G. Lutz, C.F. Rehbeg, Linear Circuit Analysis, McFraw-Hill Inc., New York, 1959.
[13] K.F. Graff, Wave Motion in Elastic Solids, Dover Publications, New York, 1991.
[14] D.L. Creedon, Y. Reshinyk, W. Farr, J.M. Martinis, T.L. Duty, M.E. Tobar, High Q-factor sapphire whispering gallery mode microwave resonator at single photon energies and millkelvin temperatures, Appl. Phys. Lett. 98 (2011) 222903.
[15] R. Morikawa, S. Ueha, K. Nakamura, Error evolution of the structural intensity measured with a scanning laser Doppler vibrometer and a k-space signal processing, J. Acoust. Soc. Am. 99 (5) (1996) 2913–2921.
[16] R. Morikawa, K. Nakamura, S. Ueha, Measuring the structural intensity by sensing the in-plane vibration, J. Acoust. Soc. Technol. 18 (4) (1997) 201–203.
[17] R. Morikawa, H. Yuzaki, K. Nakamura, S. Ueha, Ultrasonic transducer array for structural intensity measurements, Jpn. J. Appl. Phys. 35 (5B) (1996) 3080–3083.
[18] S.P. Timoshenko, Strength of Materials: Part I Elementary, third ed., Van Nostrand Reinhold Company, New York, 1955.
[19] B. Hartmann, J. Jarzynski, Ultrasonic hysteresis absorption in polymers, J. Appl. Phys. 43 (11) (1972) 4304–4312.
[20] K. Nakamae, T. Nishino, Y. Shimizu, K. Hata, Temperature dependence of the elastic modulus of crystalline regions of polyoxymethylene, Polymer 31 (10) (1990) 1909–1918.
[21] S.R. Owen, J.F. Harper, Mechanical, microscopical and fire retardant studies of ABS Polymers, Polym. Degrad. Stabil. 64 (3) (1999) 449–455.
[22] D.P. Jones, D.C. Leach, D.R. Moore, Mechanical properties of poly(ether-ether-ketone) for engineering applications, Polymer 26 (9) (1985) 1385–1393.
[23] P.J. Rae, E.N. Brown, E.B. Orler, The mechanical properties of ploy(ether-ether-ketone) (PEEK) with emphasis on the large compressive strain response, Polymer 48 (2) (2007) 598–615.
[24] H.W. Hill, D.G. Brady, Properties, environmental stability, and molding characteristics of polyphenylene sulfide, Polym. Eng. Sci. 16 (12) (1976) 831–835.
[25] S.P. Timoshenko, D.H. Young, W. Weaver, Vibration problems in engineering, fourth ed., John Wiley & Sons, New York, 1974.

Jiang Wu was born in Liaoning, China, on January 29, 1988. He received the B.E. degree in mechanical engineering from Dalian University of Technology (DUT), China, in 2010. From 2010 to 2012, he studied in the State Key Laboratory of Robotics and System, Harbin Institute of Technology (HIT), China, and received the M. E degree in mechatronic engineering from HIT in 2012. He is a presently a doctoral candidate in Precision and Intelligence Laboratory, Tokyo Institute of Technology (TITECH), Japan. His research interest includes piezoresistive and piezoelectric materials, permanent-magnet-based sensing technology, ultrasonic transducers and actuators, and ferroelectric film.

Yosuke Mizuno was born in Hyogo, Japan, on October 13, 1982. He received the B.E., M.E., and Dr.Eng. degrees in electronic engineering from the University of Tokyo, Japan, in 2005, 2007, and 2010, respectively.

From 2007 to 2010, he was engaged in Brillouin optical correlation-domain reflectometry for his Dr.Eng. degree at the University of Tokyo. From 2007 to 2010, he was a Research Fellow (DC1) of the Japan Society for the Promotion of Science (JSPS). From 2010 to 2012, as a Research Fellow (PD) of JSPS, he worked on polymer optics at Tokyo Institute of Technology, Japan. In 2011, he stayed at BAM Federal Institute for Materials Research and Testing, Germany, as a Visiting Research Associate. Since 2012, he has been an Assistant Professor at the Precision and Intelligence Laboratory, Tokyo Institute of Technology, where he is active in fiber-optic sensing, polymer optics, and ultrasonics.

Dr. Mizuno is the winner of the Funai Research Award 2010, the Ando Incentive Prize for the Study of Electronics 2011, the NF Foundation R&D Encouragement Award 2012, and the Challenging Research Award 2013. He is a member of the IEEE, the Japanese Society of Applied Physics (JSAP), and the Institute of Electronics, Information, and Communication Engineers (IEICE) of Japan.

Marie Tabaru was born in Tokyo, Japan. She received her B.Eng. degree in Electrical and Electronic Engineering from Tokyo Institute of Technology in 2002 and her M.E. degree in Human System Science in 2005. She studied image signal processing of medical ultrasound at the University of Washington, Seattle, WA from 2002 to 2003. She received the Best Student Paper Award in Engineering Acoustics from the Acoustical Society of America in 2006. She received her D.E. degree from Tokyo Institute of Technology in 2007. She has been an associate professor of the Precision and Intelligence Laboratory, Tokyo Institute of Technology since 2013. She is a member of the Acoustical Society of Japan, the Japan Society of Ultrasonics in Medicine, and the Institute of Electronics, Information and Communication Engineers.

Kentaro Nakamura was born in Tokyo, Japan, on July 3, 1963. He received the B.E., M.E., and Dr.Eng. degrees from Tokyo Institute of Technology, Japan, in 1987, 1989, and 1992, respectively.

Since 2010, he has been a Professor at the Precision and Intelligence Laboratory, Tokyo Institute of Technology. His research field is the applications of ultrasonic waves, measurement of vibration and sound using optical methods, and fiber-optic sensing.

Prof. Nakamura is the winner of the Awaya Kiyoshi Award for encouragement of research from the Acoustical Society of Japan (ASJ) in 1996, and the Best Paper Awards from the Institute of Electronics, Information and Communication Engineers (IEICE) in 1998 and from the Symposium on Ultrasonic Electronics (USE) in 2007 and 2011. He also received the Japanese Journal of Applied Physics (JJAP) Editorial Contribution Award from the Japan Society of Applied Physics (JSAP) in 2007. He is a member of the IEEE, the ASJ, the JSAP, the IEICE, and the Institute of Electrical Engineers of Japan (IEEJ).